J. Phys. D: Appl. Phys. **31** (1998) 159–164. Printed in the UK PII: S0022-3727(98)79460-4

Nondestructive determination of sheet carrier density in pseudomorphic AlGaAs/InGaAs/GaAs high electron mobility transistor structures by room-temperature photoluminescence spectra

Wu Lu†‡, Jin-Hee Lee§, Krishnamachar Prasad†, Geok-Ing Ng† and Per Lindström‖

† Microelectronics Center, School of Electrical and Electronic Engineering, Nanyang Technological University, Singapore 639798
§ Compound Semiconductor Devices Section, Electronics and Telecommunications Research Institute, Taejon 305-350, Korea
‖ Department of Computer Science, Umeå University, Umeå, Sweden

Received 11 November 1996, in final form 30 May 1997

Abstract. This paper describes a nondestructive method to determine the sheet carrier density of pseudomorphic high electron mobility transistor structures by fitting the room-temperature photoluminescence (PL) spectra. The sheet carrier densities determined were in sufficiently good agreement with values determined by Hall measurements for different samples with different mole fractions, δ-doping densities and well widths. For single-doped AlGaAs/InGaAs quantum wells, the dominant emission is the transitions from the first electron subband to the first heavy hole subband, from the first electron subband to the second heavy hole subband, and from the second electron subband to the first heavy hole subband.

1. Introduction

Photoluminescence (PL) is a useful tool for investigating material growth quality and impurity concentration in bulk materials [1, 2]. Modulation-doped quantum wells (MDQWs) exhibit several interesting features from both fundamental research and application viewpoints. Pseudomorphic high electron mobility transistors (pHEMTs) based on an AlGaAs/InGaAs quantum well system have demonstrated their high potential for low-noise, microwave power, and high-speed digital applications [3–5]. The performance of a pHEMT depends on the two-dimensional electron gas (2DEG) which is formed by a large number of electrons confined in the InGaAs channel layer. Usually the sheet carrier density is determined by Hall or Shubriko–de Haas (SdH) measurements. However, separately fabricated samples with Ohmic contacts are necessary for Hall and SdH measurements. Investigations of the correlation between such electrical properties and optical properties, which are determined by nondestructive optical measurements, have therefore attracted much interest.

The InGaAs QW makes PL a valuable tool to investigate the 2DEG because it greatly enhances the PL efficiency due to the strong wavefunction overlap of electrons and holes. Dodapur *et al* [6] demonstrated that the PL linewidth at 77 K was a good measure of the sheet carrier density in an AlGaAs/InGaAs/GaAs material system. Brugger *et al* [7] established a relation between the sheet carrier density and the energy separation between the high-energy intensity cutoff and the intensity maximum of the first spectral band of PL spectra at 20 K, which was in good agreement with SdH results in the range of 1.1 to 2.6×10^{12} cm^{-2}. At higher concentrations up to 4.0×10^{12} cm^{-2}, Brierley *et al* [8] demonstrated a correlation between the sheet carrier density and the width of the second subband PL peak at 77 K. All the above mentioned works were based on low-temperature PL spectra. Though it is not impossible to measure a large sample at 77 K or lower temperatures, an easy nondestructive method to determine the sheet carrier density using room-temperature PL spectra

‡ To whom correspondence should be addressed.

n^+-GaAs 5×10^{18} cm^{-3}	500 Å
i-$Al_xGa_{1-x}As$	400 Å
Si δ-doped plane	
i-$Al_xGa_{1-x}As$	30 Å
i-$In_yG_{1-y}As$	120~150 Å
i-GaAs	6000Å
S/L	GaAs/AlAs
S. I.	GaAs substrate

Figure 1. Cross sectional structure of a pHEMT.

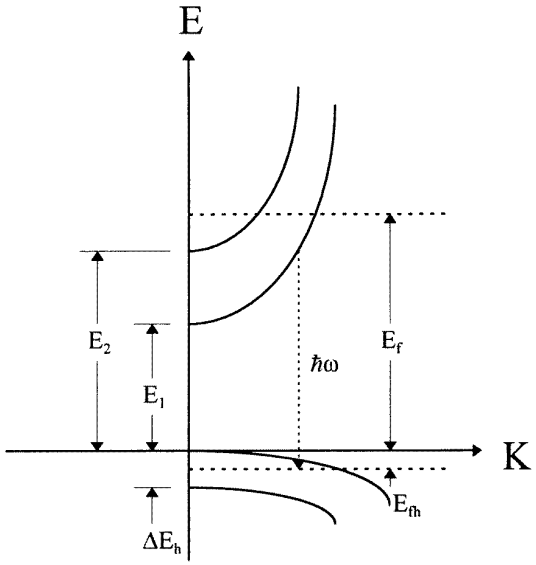

Figure 2. Schematic in-plane band structure of an AlGaAs/InGaAs strained quantum well in which the first two electron subbands and the first heavy hole subbands are shown.

is desired by device engineers. However it is difficult to apply the methods mentioned above to room-temperature PL spectra because of the strong overlap of emissions from different subband energy transitions and various broaden mechanisms.

In this work, through a detailed line-shape analysis, we investigate the relationship between sheet carrier density and room-temperature PL spectra of pHEMT structures. It is demonstrated that sheet carrier density information can be deduced from such PL line-shape analyses.

2. Experimental details

The samples in our study were grown by molecular beam epitaxy (MBE) in a Riber MBE45 system. A typical structure of the samples is shown in figure 1 and consists of the following layers grown sequentially, from bottom to top, on a semi-insulating GaAs substrate: 6000 Å GaAs with ten superlattices of AlAs/GaAs as a buffer layer; undoped InGaAs strained layer; AlGaAs spacer; Si δ-doped plane; 400 Å i-AlGaAs source layer; and a Si-doped 500 Å n^+-GaAs cap layer. The individual structural parameters of five samples used are shown in table 1. The growing layer thickness and compositions were determined by reflection high-energy electron diffraction (RHEED) oscillations. Before Hall and PL measurements, the cap layer of the samples was etched to 50 Å for the fabrication of Ohmic contacts for Hall measurements.

For PL measurements, excitation was provided by the 514.5 nm line from an Ar^+ laser at a typical power density of $\sim$5 W cm^{-2}. At the higher temperatures of interest in this work, significantly stronger excitation is required with the corresponding photogeneration of more holes so that holes are available over a substantial energy range. The emission signal from the sample was detected and amplified by a cooled InGaAs pin photodiode and a lock-in amplifier. Hall measurements were performed at room temperature to determine the sheet carrier density for comparison.

3. PL data analysis

Figure 2 shows the first several subbands of the in-plane band structure of an AlGaAs/InGaAs quantum well. The line-shape model used for fitting the measured PL spectra is based on the following assumptions: (1) nonparabolicity is sufficiently small to be neglected; (2) only transitions relative to heavy hole subbands are considered; (3) four optical transitions—from the first electron subband to the first heavy hole subband, from the first electron subband to the second heavy hole subband, from the second electron subband to the first heavy hole subband, and from the second electron subband to the second heavy hole subband, designated (E_1–HH_1), (E_1–HH_2), (E_2–HH_1) and (E_2–HH_2) respectively—are included. The PL behaviour of a degenerate electron gas has been studied by Lyo and Jones [9] in modulation-doped n- and p-type QWs. The intensity of the direct optical transition between an electron and a hole subband at a particular wave vector is determined by considering the density of states of electrons and holes and the respective occupation probabilities of the two subbands at the given wave vector. The total PL intensity for the structure we investigated, which has been accurately described by Brierley [10] as a function of photon energy, is

$$I(\bar{h}\omega) = \sum_{i,j} B_{ij} D(\bar{h}\omega) g_{ei}(\bar{h}\omega) g_{hj}(\bar{h}\omega) \qquad (1)$$

where B_{ij} are numerical coefficients, i and j are the various electron and heavy hole subband indices, $D(\bar{h}\omega)$ is the broadened density of states step function which is represented by

$$D(\bar{h}\omega) = \frac{1}{1+\exp[-(\bar{h}\omega - E_g)/\Gamma)]} \qquad (2)$$

where E_g is the energy gap separating the two subbands and Γ is a broadening parameter, $g_e(\bar{h}\omega)$ is the occupancy of

Table 1. Samples used and their structural parameters.

Sample	Al	In	Well width (Å)	Spacer layer (Å)	Si δ-doping (10^{12} cm^{-2})	Source layer (Å)	Cap layer (Å)
A	0.24	0.15	150	30	4.5	400	500
B	0.24	0.20	120	30	4.5	400	500
C	0.24	0.15	120	30	4.5	400	500
D	0.24	0.15	120	30	3.0	400	500
E	0.24	0.15	120	30	6.0	400	500

the electron subband, which is the Fermi–Dirac distribution function of electrons given by

$$g_e(\hbar\omega) = (1 + \exp(\{[m_h/(m_e + m_h)]\hbar\omega + [m_e/(m_e + m_h)]E_g - E_F\}/\mathrm{kT}))^{-1} \quad (3)$$

where m_e and m_h are the effective masses of electrons and heavy holes respectively, E_F is the Fermi level, T is the lattice temperature and k is the Boltzmann constant. Similarly, $g_h(\hbar\omega)$ is the hole occupation probability, which is described by

$$g_h(\hbar\omega) = [\![1 + \exp(\{[m_e/(m_e + m_h)] \times (\hbar\omega - E_g) - E_{Fh}\}/kT)]\!]^{-1} \quad (4)$$

where E_{Fh} is the quasi-Fermi level for holes [10].

Equations (1)–(4) are used to fit the observed PL spectra, adjusting B_{ij}, electron subband energies E_i, E_F, Γ_i, E_{Fh}, and an offset as fitting parameters by the Gauss–Newton method to solve the constrained nonlinear least-squares problems. From the fitted parameters, the sheet carrier density can be determined from [11]

$$n_s = \frac{kTm_e}{\pi\hbar^2} \sum_i \ln\left[1 + \exp\left(\frac{E_F - E_i}{kT}\right)\right] \quad (5)$$

where E_i is the ith electron subband energy.

4. Results and discussion

Figure 3 shows the room temperature PL spectrum (full curve) of sample E. From which only one peak and one shoulder can be clearly observed. Because of various homogeneous and inhomogeneous broadening mechanisms at room temperature, the spectrum is broadened and overlapped and As a result it is difficult to determine the dominant transitions. It is also quite difficult to ascertain the transition energy, intensity and the full width at half maximum (FWHM) of every peak. In general, low- temperature PL measurements have to be taken to determine the energy levels accurately. In figure 3, the broken curve is the fit of the room-temperature spectrum of sample E. This is the sum of three peaks with intensities I_{11}, I_{12}, I_{21} which means the dominant emission consists of (E_1–HH_1), (E_1–HH_2), and (E_2–HH_1) transitions. The agreement between the PL spectrum and its fit in figure 3 is quite good. The fitting result also demonstrates that there is no emission relative to the (E_2–HH_2) transition, which can be explained by the fact that band bending yields a triangular potential in which parity-allowed transitions are unfavourable. The determined subband energies are 1.217 eV and 1.294 eV. Accordingly, the PL determined sheet carrier density is 2.17×10^{12} cm^{-2}, which is close to the data determined by Hall measurements, 2.15×10^{12} cm^{-2}. Fits for the PL spectra of samples B, C, and D also showed that the fits were composed of (E_1–HH_1), (E_1–HH_2), and (E_2–HH_1) transitions. However, sample A showed only (E_1–HH_2) and (E_2–HH_1) transitions. This characteristic originates from the differences in (HH_1–HH_2). The fitted values of (HH_1–HH_2) are respectively 14, 30, 29, 28 and 32 meV for structures A, B, C, D and E. The degree of the hole thermal excitation depends on the value of (HH_1–HH_2). Figure 4 shows a comparison of sheet carrier densities of several samples determined by Hall and PL methods. The sheet carrier densities calculated from the fits of room-temperature PL spectra to the model show good agreement with data determined by Hall measurements, especially in the density range of 2.0×10^{12}–3.0×10^{12} cm^{-2}, which is typical of the structures in practical pHEMT applications.

The differences between the sheet carrier densities determined by the two methods are to be expected for a number of reasons. For instance, transitions relative to the third or higher subband energy levels are not included in our calculations. As a result, the optically determined values do not include the number of electrons which occupy the third or higher subbands, though a very few electrons do occupy these subbands. Second, the emission from buffer layers, which is centred at 1.423 eV, is very much weaker than the emission from the quantum well and is far away from the (E_2–HH_1) transition. Sometimes, however, it overlaps the (E_2–HH_1) transition and in this case a signal processing technique is necessary to filter the buffer layer emission from the PL spectrum. Third, Hall measurements were used as the reference for our PL analysis, which of course also normally contain errors.

Fitting results actually yield more information than just energy levels and sheet carrier densities. From the curve-fitting results, we can also determine the peak position, intensity and FWHM of each peak accurately and these are listed in table 2. Another important parameter is the localized energy of holes, which describes the extent of hole localization. From the fit, the hole localized energy of sample A is 0.15 eV, which corresponds to a hole localized radius of 81.8 Å at room temperature. Moreover, for structures C, D and E, which are identical apart from their δ-doping densities, although the fitting results show that the PL spectrum is composed of the same transitions, the corresponding relative intensities I_{11}, I_{12}, and I_{21} are very different. As shown in figure 5, I_{11}/I_{12} and I_{11}/I_{21} change

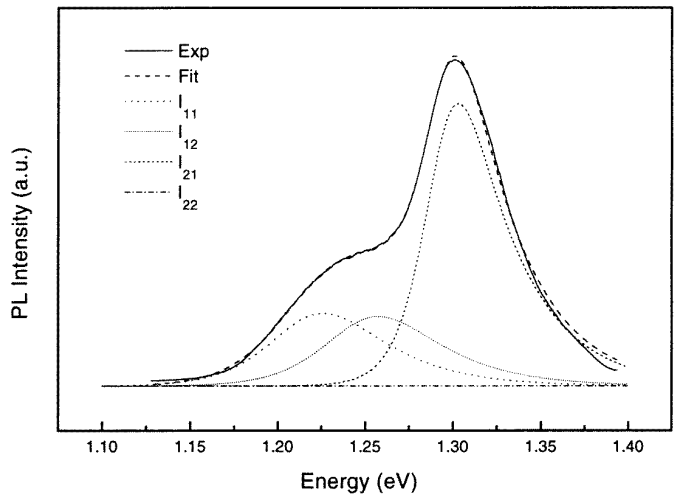

Figure 3. Room-temperature photoluminescence spectrum of sample E and its fit to the model.

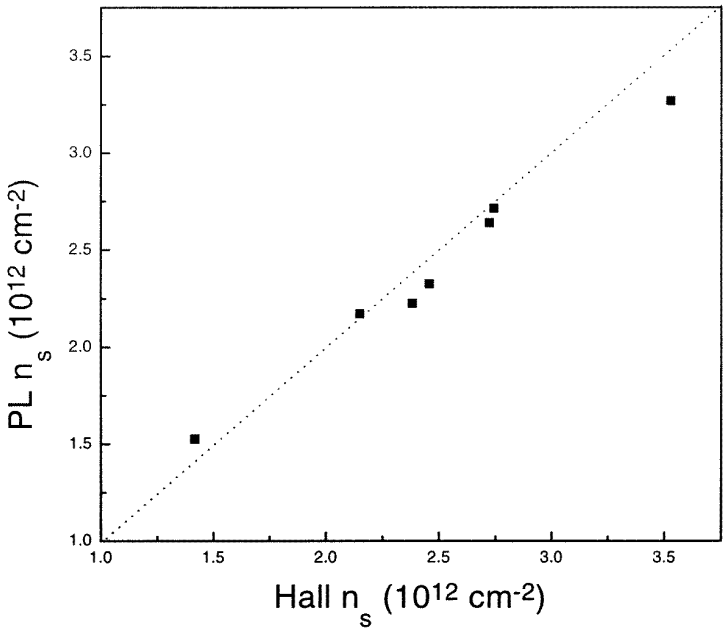

Figure 4. Comparisons of the sheet carrier densities calculated from the fits to room-temperature PL spectra and the sheet carrier densities determined by Hall effect measurements for the samples in this study. The broken unity-slope line is shown for reference.

Table 2. Intensities (I_{ij}), peak positions (P_{ij}), and FWHMs (W_{ij}) of different transitions determined from the fitting results.

Sample	I_{11} (a.u.)	P_{11} (eV)	W_{11} (meV)	I_{12} (a.u.)	P_{12} (eV)	W_{12} (meV)	I_{21} (a.u.)	P_{21} (eV)	W_{21} (meV)	I_{22} (a.u.)	P_{22} (eV)	W_{22} (meV)
A	0	—	—	4.74	1.222	93	16.79	1.265	51	0	—	—
B	15.48	1.220	79	6.231	1.251	77	28.32	1.289	53	0	—	—
C	10.51	1.230	67	6.17	1.260	66	23.58	1.299	50	0	—	—
D	29.84	1.233	59	9.43	1.261	58	40.81	1.296	53	0	—	—
E	3.27	1.226	76	3.12	1.258	76	12.70	1.303	53	0	—	—

significantly with increasing δ-doping density whilst I_{12}/I_{21} is almost constant.

To investigate this feature we calculated the separation changes of conduction subband levels and valance subband

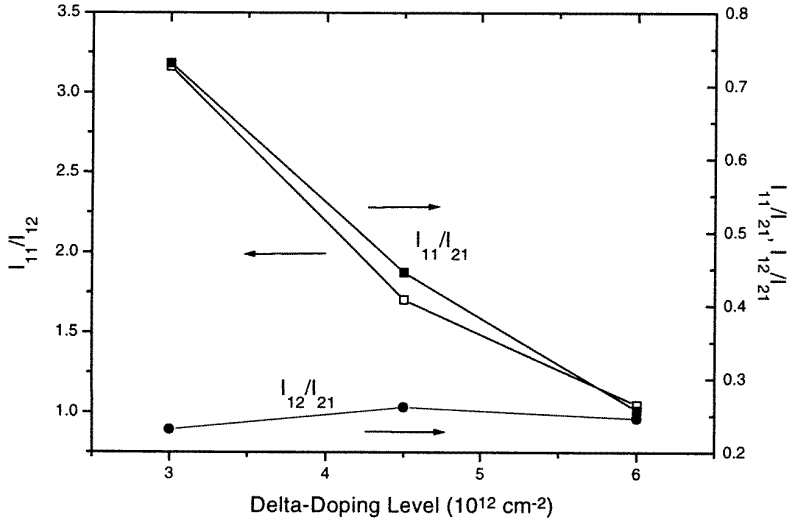

Figure 5. Comparisons of relative intensities of (E_1–HH_1), (E_1–HH_2), and (E_2–HH_1) dependence of δ-doping levels.

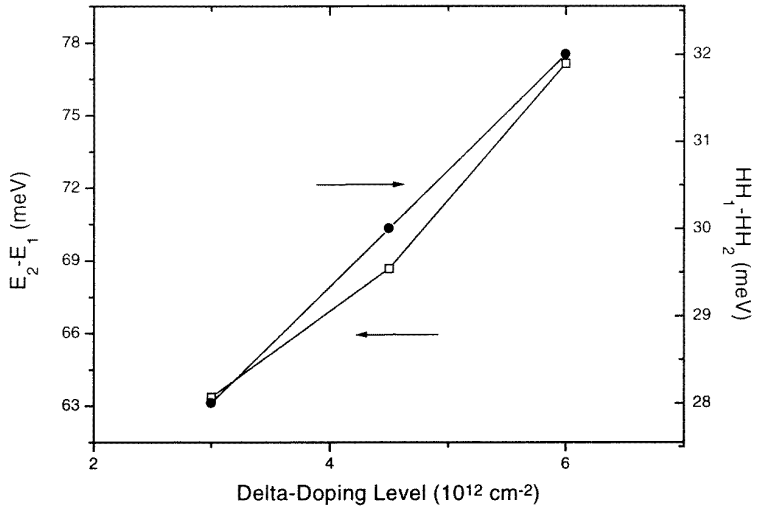

Figure 6. Dependence on δ-doping level of separations of the first two electron subbands and the first two heavy hole subbands which are calculated from fits to the model.

levels, E_2–E_1 and HH_1–HH_2, which are shown in figure 6. As above mentioned, for the structures investigated here, nonparity transitions are preferred because of band bending which yields a triangular potential. Figure 6 shows that with an increase of δ-doping level from 3.0×10^{12} cm^{-2} to 6.0×10^{12} cm^{-2}, the change in the separation of the first two electron subbands is 15 meV and that the first two heavy hole subbands is only about 4 meV. As the δ-doping level increases and hence electrons are confined in the channel layer, band bending increases. When $E_F > E_2$ with increased sheet carrier concentration, the shape of the QW becomes sharper. The overlap between the E_1 and HH_1 wavefunctions then decreases and the overlap between the E_2 and HH_1 wavefunctions increases. Conversely, as the sheet carrier concentration in the well decreases, band bending decreases. Then, the QW flattens and the overlap between the E_1 and HH_1 wavefunctions increases whereas the overlap between the E_1 and HH_2 wavefunctions decreases. In another aspect, the value of (HH_1–HH_2) determines the degree of hole thermal excitation and hence the population of holes in the HH_2 subband. A slightly increasing tendency of I_{12}/I_{21} is clearly observed, which can be attributed to the increase in hole population in the HH_2 subband because of the slight increase in the value of (HH_1–HH_2).

5. Summary

In summary, we have demonstrated a nondestructive method to determine the sheet carrier densities of AlGaAs/InGaAs HEMT structures by the fitting of room-temperature PL spectra. For the samples used here, our results show sufficiently good agreement with the values determined by Hall measurements. The method

can be used for the determination of sheet carrier density for pHEMT structures prior to device fabrication. The calculation results also show that the dominant emission of a single-side-doped AlGaAs/InGaAs quantum well is that from (E_1–HH_1), (E_1–HH_2) and (E_2–HH_1) transitions. The fitting results also yield important information on the peak position, FWHM, the intensity of each transition, subband energies, and the hole localized energy. The relative intensity of the (E_1–HH_1) and (E_1–HH_2) transitions is sensitive to the separation of heavy hole subbands, which describes the degree of hole thermal excitation. For single-side-doped AlGaAs/InGaAs quantum wells, transitions with different electron and hole subband indices, i.e. forbidden pairs, are preferred.

Acknowledgments

The authors are indebted to Dr Hae-Gwon Lee for sample growth, Dr Seung-Won Lee for PL measurements and D Chul-Soon Park for beneficial discussions.

References

[1] Pearsall T P, Eaves L and Portal 1983 *J. Appl. Phys.* **54** 1037
[2] Livescu G, Miller D A B, Chemla D S, Ramaswamy M, Chang T Y, Sauer N, Gossard A C and English J H 1988 *IEEE J. Quant. Electron.* **24** 1677
[3] Lee J H, Yoon H S, Park C S and Park H M 1995 *IEEE Electron Device Lett.* **16** 271
[4] Smith P, Chao P, Ballingall J and Swansen A 1990 *Microwave J.* **33** 71
[5] Abe M and Mimura T 1991 *IEEE J. Solid State Circuits* **26** 1337
[6] Dodabalapur A, Kesan V P, Neikirk D P, Streetman B G, Hermam M H and Ward I D 1990 *J. Electron. Mater*. **19** 265
[7] Brugger H, Mussig H, Wolk C, Kern K and Heitmann D 1991 *Appl. Phys. Lett.* **59** 2739
[8] Brierley S K, Hoke W E, Lyman P S and Hendriks H T 1991 *Appl. Phys. Lett.* **59** 3306
[9] Lyo S K and Jones E D 1998 *Phys. Rev.* B **38** 4113
[10] Brierley S K 1993 *J. Appl. Phys.* **74** 2760
[11] Jogai B, Yu P W and Streit D C 1994 *J. Appl. Phys.* **75** 1586